Hindawi
International Journal of Forestry Research
Volume 2022, Article ID 8103242, 14 pages
https://doi.org/10.1155/2022/8103242

Research Article

AMMI Automatic Mangrove Map and Index: Novelty for Efficiently Monitoring Mangrove Changes with the Case Study in Musi Delta, South Sumatra, Indonesia

Suyarso and Praditya Avianto

Research Center for Oceanography, National Research and Innovation Agency, Jakarta, Indonesia

Correspondence should be addressed to Suyarso; suyarso.nana.lipi@gmail.com

Received 10 March 2022; Revised 26 September 2022; Accepted 5 October 2022; Published 8 December 2022

Academic Editor: Ranjeet Kumar Mishra

Mapping mangroves using satellite imagery has been done for decades. It helps reduce obstacles in inaccessible places caused by the mangroves' intricate root system, thick mud, and loss of position signals. There is an urgent need to produce a mangrove map that automatically and accurately covers the mangroves with the density index of the canopy as visually represented in satellite imagery. The research was conducted through an analytical desk study of the mangrove features from space. The study aims to develop a simple formula for automatically tracing, capturing, and mapping mangroves and determining the canopy density index from open access of satellite data to eliminate manual digitization work, make it easy to use, and save cost and time. The goal is to monitor, assess, and manage the condition of mangroves for anyone interested in mangroves, including the central government, local authorities, and local communities. As a result, the authors proposed an algorithm: $(\rho_{NIR} - \rho_{Red})/(\rho_{Red} + \rho_{SWIR1}) * (\rho_{NIR} - \rho_{SWIR1})/(\rho_{SWIR1} - 0.65 * \rho_{Red})$. Experimental results in many mangrove forests using Landsat 5 TM, Landsat 7 ETM, Landsat 8 OLI, and Sentinel 2 imageries show satisfactory performance. The maps capture the spatial extent of the mangroves automatically and match the satellite imagery visually. The index correlates significantly with the Normalized Difference Water Index (NDWI), with R^2 reaching 0.99. The research will apply the formula of the Musi Delta mangrove complex in South Sumatra, Indonesia. The advantage of the algorithm is that it works well, is easy to use, produces mangrove maps faster, informs the index, and efficiently monitors the change in mangrove conditions from time to time.

1. Introduction

Mangroves are woody plants that grow inland and at the marine boundary (coastal), especially in tropical and subtropical areas [1, 2]. Mangrove ecosystems are characterized by high environmental dynamics, e.g., temperature, sedimentation, and tidal currents [3]. Mangroves are highly beneficial to coastal ecosystems and shallow waters due to their contribution to the coastal zone, productivity, and biologically essential ecosystems [4]. The environment has specific characteristics that are generally influenced by freshwater from the land via rivers and saltwater from the sea [5, 6]. The mangrove ecosystem provides services such as nursery areas for many marine fisheries and nutrient cycling [7], habitat for wildlife species, the landing site for thousands of migratory birds [3], and biodiversity [8]. In the context of climate change, mangroves play an important role in carbon sequestration as they can sequester carbon in the atmosphere through photosynthetic processes, and most of them are also stored in the soil [9–14].

Mangroves are vulnerable to anthropogenic and natural disturbances. The Food and Agriculture Organization of the United Nations (FAO) [15] reports that 20% of the world's mangroves have been lost to deforestation since the 1980s. Anthropogenic factors that play a significant role include urban expansion [16–21], functional change to aquaculture and shrimp farming [22], illegal exploitation for fuelwood and construction materials [23], or damage from natural factors such as storms, hurricanes, and tsunamis [24, 25].

The world's attention is now focused on climate change, where the physical manifestations of threats are often referred to as hazards or climate hazards [26] and rising sea levels significantly impact coastal environments. Most mangroves do not keep pace with sea level rise because sediments are not as high and a limited area is available for landward migration [27]. In tropical countries where mangrove forests thrive, Sierra-Correa and Kintz [28] emphasized that the long-term threat of sea level rise requires coastal planning to avoid much more significant losses.

The Indonesian Minister of Environment and Forestry's opening speech at the International Conference on Sustainable Mangrove Ecosystems in BAli on April 18, 2017 [29] states that Indonesia has a mangrove ecosystem area of 3.5 million hectares. The government manages 2.2 million hectares, and communities manage the remaining 1.3 million hectares, located in 257 districts/cities, most of which are degraded.

For decades, remote sensing via satellite imagery has been widely used to monitor the condition of mangroves. Its ability to cover broader areas and its temporally make it ideal from time to time [30–32], and more than 1300 scientific remote sensing papers on mangroves have been published on various topics [33]. Mapping mangroves with multispectral, medium-resolution images is the most popular data source. Landsat 8, launched on February 11, 2013, has 11 bands, with the spatial resolution of the panchromatic band being 15 m. Sentinel-2A was launched on June 23, 2015, and Sentinel-2B was launched on March 7, 2017. Both provide 13 multispectral bands with a spatial resolution of 10 m for vegetation detection. Compared to previous Landsat satellites, the beam resolution was increased to 16 bits, and the signal-to-noise ratio was significantly improved. These advances improved Landsat 8's ability to discriminate vegetation [34]. These satellite images are easy to collect and open to access, and free software is now available to support image processing. However, the problem is that the results of mangrove research using remote sensing have stagnated at only the journal level for academics and researchers. It is difficult for interested practitioners and local communities to apply the results.

This research aims to develop a simple formula to automatically trace, capture, and map mangroves and inform the index based on satellite imagery. The goal is to monitor, assess, and manage the mangrove condition, and this can be performed by anyone interested in mangroves, including the central government, local government, and local communities. With the requirements of the next 10–15 years, the mapping of mangroves will cover a larger area. Google Earth Engine (GEE) is a platform that provides multitemporal satellite image data archives. The platform provides applications for various user-created formulas, allowing the possibility of using an algorithm to access mangroves [35, 36]. Collecting satellite imagery through the GEE helps users remove clouds, is free from mosaic processes, and is not limited in its spatial coverage.

Technically, AMMI creates an effective and efficient mangrove map that eliminates traditional work such as manual digitization or other classical classification methods. Scientifically, automatic mangrove mapping can cover a much broader area more quickly. Therefore, this method will provide information not only on the presence and spatial extent of mangroves but also inform the relationship of mangroves to coastal geomorphology [37] and their ecological conditions [31], which can eventually be used to determine and assess the health status of mangroves.

The case study is near the Musi River Delta in South Sumatra Province, Indonesia (Figure 1). The area is administratively divided into two parts. The northwestern part is a small part of the Sembilang National Park (SNP) under the central government's control. The other southeastern part is the Air Telang Protected Forest (ATPF) under the control of the South Sumatra provincial government.

2. Material and Methods

2.1. Material. The materials used for the study are medium-resolution optical satellite images that are open access, such as Landsat 5 TM, Landsat 7 ETM, Landsat 8 OLI, and Sentinel 2. The data used are listed in Table 1, and the data characteristics are shown in Table 2 below.

2.2. Methods

2.2.1. Images Processing. Images processing consists of several steps: radiometric calibration, which is converted from the digital number (DN) to a ToA (top of atmospheric) value, pan-sharpening, i.e., the fusion of band 2–band 7 with a resolution of 30 m × 30 m through a panchromatic band 8 with a resolution of 15 m × 15 m, image stacking, and image resizing of the images. The following equation shows the formula to convert the digital number to the surface reflectance:

$$\rho_\lambda = \frac{M\rho Q_{cal} + A\rho}{\sin(\theta_{SUN})}, \quad (1)$$

where, ρ_λ: real reflectance on the earth surface, $M\rho$: band-specific multiplicative rescaling factor, Q_{cal}: Quantized and calibrated standard product pixel values (DN), $A\rho$: band-specific additive rescaling factor, and θ_{SUN}: local sun elevation angle

All the above parameters are stored in the MTL file of each image packet. The real reflections as results of the processing of L and sat and Sentinel images are annotated as ρ_{Blue}, ρ_{Green}, ρ_{Red}, ρ_{NIR}, ρ_{SWIR1}, and ρ_{SWIR2} for *Blue*, *Green*, *Red*, *NIR*, *SWIR1*, and *SWIR2*, respectively. In Landsat 8 OLI, a panchromatic band increases the spatial resolution to 15 m. The result of the fusion, due to the higher spatial resolution, makes the image visually clearer [38]. However, the color pattern still obtained images with a resolution of 30 m × 30 m [39]. A panchromatic band increases spatial resolution, and spatial sharpening will be visually helpful in interpreting the mangrove [34]. This work converts the digital number of images into surface reflectance for radiometric correction using DOS1 in the semiautomatic classification plugin (SCP) module in QGIS vers. 3.4 Madeira.

Figure 1: The case study is located in the Musi River delta, South Sumatra, Indonesia.

Table 1: Multitemporal images from Landsat 5 TM, Landsat 7 ETM, Landsat 8 OLI, and Sentinel 2 were used for the study, along with the percentage of clouds and shadows in the study area.

No	*Date of record*	*Bundle of landsat 8 OLI*	*Clouds and shadows cover (%)*
1	September 9, 2019	LC08_L1TP_124062_20190909_20190917_01_T1.tar	14.0
No	*Date of record*	*Bundle of landsat 7 ETM*	*Clouds and shadows cover (%)*
1	June 30, 2002	LE07_L1TP_124062_20020630_20170130_01_T1.tar	3.0
2	September 13, 2012	LE07_L1TP_124062_20120913_20161129_01_T1.tar	15.0
3	October 13, 2011	LE07_L1TP_124062_20111013_20161206_01_T1.tar	18.0
No	*Date of record*	*Bundle of landsat 5 TM*	*Clouds and shadows cover*
1	May 17, 1989	LT05_L1TP_124062_19890517_20170203_01_T1.tar	5.0
No	*Date of record*	*Bundle of sentinel 2*	*Clouds and shadows cover*
1	July 16, 2021	L1C_T48MVC_A031675_20210716T032022	15.0

Table 2: Correlation and equivalence of bands in Landsat 5 TM, Landsat 7 ETM, Landsat 8 OLI, and Sentinel 2 imageries.

Landsat 5	Landsat 7	Landsat 8 OLI			Description	Sentinel 2		
Band	Band	Band	Resolution (m)	Wavelength (μm)		Band	Resolution (m)	Wavelength
1	1	2	30	0.450–0.515	Blue	2	10	0.443
2	2	3	30	0.525–0.600	Green	3	10	0.490
3	3	4	30	0.630–0.680	Red	4	10	0.560
4	4	5	30	0.845–0.885	Near infraRed (NIR)	8A	20	0.865
5	5	6	30	1.560–1.660	Short wave infraRed 1 (SWIR1)	11	20	1.610
7	7	7	30	2.100–2.300	Short wave infraRed 2 (SWIR2)	12	20	2.190

2.2.2. Spectral Characteristics of Mangroves on Satellite Images. Leaf structure can be identified using narrow bandwidth spectroradiometers in the visible (ρ_{Blue}, ρ_{Green}, and ρ_{Red}) and ρ_{NIR} of the spectrum. In the visible range (400–700 nm), leaf structure is low due to the absorption of photosynthetic pigment (chlorophylls and carotenoids). In the ρ_{NIR} domain (700–1300 nm), where there is no strong absorption, the magnitude of reflectance is governed by the structural discontinuities encountered in the leaf. The ρ_{SWIR} region (1300–3000 nm) presents variable values, mainly linked to the absorption characteristics of water and other compounds. Thus, the ρ_{Red} edge, the wavelength of

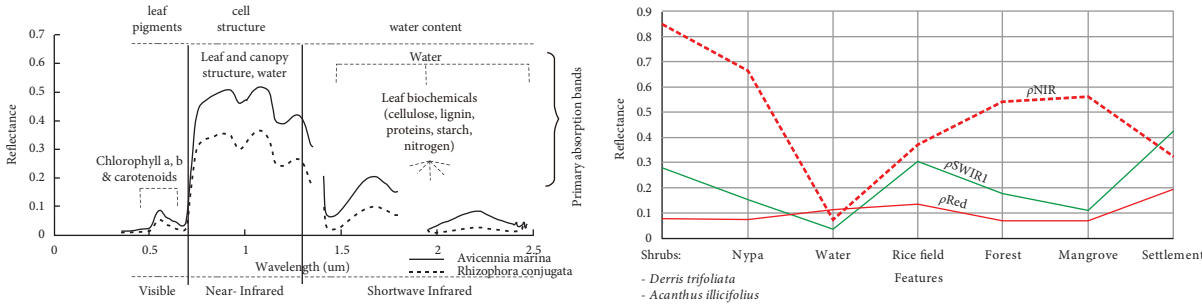

(a) (b)

Figure 2: (a) Spectral characteristics and their influencing parameters of the mangrove species of *Avicennia marina* and *Rhizophora conjugate* [31]. (b) The reflectances (ρ_{Red}, ρ_{NIR}, and ρ_{SWIR1}) representatives were collected from various land covers in Segara Anakan mangrove forests in Cilacap, Central Java, Indonesia. (Shrubs are *Derris trifoliate* and *Acanthus illicifolius*).

maximum slope in the increase of reflectance from ρ_{Red} to ρ_{NIR} has been a good indicator of the leaf level's chlorophyll content and at the canopy level [40, 41].

Kuenzer et al. [31] and [42] found that the spectral response of mangroves in the wavelength range of 380–750*n*m ($\rho_{Blue} - \rho_{Red}$) is feeble, while it is strong in the spectrum of 750–2500 nm ($\rho_{NIR} - \rho_{SWIR2}$), especially concerning to leaf structure and properties, water content, and mangrove biochemistry. An illustration of the spectral response in mangroves is shown in Figure 2(a). The visible reflectance is lower than in ρ_{NIR} due to chlorophyll absorption and leaf cell wall scattering. Further explained, the reflectance of ρ_{NIR} is principally controlled by the walls of the spongy mesophyll cells, with healthier leaves tending to have more substantial reflectance in ρ_{NIR} as they reflect excessive amounts of incoming energy from the electromagnetic spectrum. In contrast, stressed leaves will have lower reflectance due to cell structure changes. The leaf water content is the primary determinant of reflectance in the ρ_{SWIR} region.

From the reviews above, it is generally accepted as the basic principles of the optical-remotely sensed to detect vegetation: chlorophyll-based, sensitive in the $\rho_{Red} - \rho_{NIR}$ wavelength range and water content-based in leaves which are sensitively in the $\rho_{NIR} - \rho_{SWIR1}$ wavelength range. Many formulas have been available in mangrove research, probably almost a hundred, as revealed by Xue and Su [43] and Kobayashi et al. [44]. Even though the revealed formulas cannot automatically delineate mangroves, manual digitization is still used in mangrove research to separate mangroves and other features. As is known, the work is very tedious, tiring, and time-consuming.

The existing vegetation indices (VIs) can be broadly grouped into two main streams: (1) the chlorophyll-based content of the vegetation with all its variants, and (2) the water/moisture-based content with all its variants.

2.2.3. The Existing Vegetation Indices as References

(1) Formula Based on Chlorophyll Content. Healthy vegetation based on chlorophyll content reflects more ρ_{NIR} and ρ_{Green} light than other wavelengths and absorbs more red and blue light. As an indicator of health, chlorophyll strongly absorbs visible light, and the cell structure of leaves strongly reflects ρ_{NIR}. When the plant is dehydrated, diseased, or affected by a disease, the sponge layer deteriorates and the plant absorbs more near-infraRed light instead of reflecting it. Thus, observing how ρ_{NIR} changes compared to ρ_{Red} provides an accurate indication of the presence of chlorophyll, which correlates with plant health. Stressed mangroves have greater reflectance in visible light, particularly in the ρ_{Red} regions, likely due to a decrease in chlorophyll content and an increase in carotenoids in the leaves [42].

There are formulas, the oldest and simplest of which, the ratio vegetation index (RVI) using ρ_{Red} and ρ_{NIR}, was formulated as (ρ_{Red}/ρ_{NIR}) proposed by Jordan [45]. The RVI is widely used for estimating and monitoring green biomass, especially when there is a dense vegetation cover. This index is sensitive to vegetation and correlates with plant biomass. However, when vegetation cover is sparse (less than 50%), the RVI is more sensitive to atmospheric effects, and its representation of biomass is weak [44].

The most popular is the normalized difference vegetation index (NDVI) proposed by Rouse et al. [46], which has been the most common and widely used in mangrove remote sensing for more than two decades [41, 47]. NDVI quantifies vegetation by measuring the difference between ρ_{NIR} (which is strongly reflected by vegetation) and ρ_{Red} (which is absorbed by vegetation), formulated as $(\rho_{NIR} - \rho_{Red})/(\rho_{NIR} + \rho_{Red})$. NDVI was initially developed to monitor plant growth in plantation environments. However, this formula is adopted and applied in mangrove research. It is estimated that this formula has been used and applied in hundreds of mangrove research papers.

Several derivatives of NDVI have also been proposed to address the limitations, including the perpendicular vegetation index (PVI) [48], the soil-adjusted vegetation index (SAVI) [49], the atmospherically resistant vegetation index (ARVI) [50], and the global environment monitoring index (GEMI) [51]. These attempted to incorporate intrinsic corrections for one or more confounding factors. Several new generation algorithms are proposed for estimating biogeophysical variables to take advantage of modern sensors' improved performance and characteristics and eliminate confounding factors. Despite these factors, NDVI

remains a valuable tool for quantitatively monitoring vegetation in terms of photosynthetic capacity at a spatial scale appropriate for various phenomena.

(2) Formula Based on Water/Moisture Content. The Infrared Index (II) was proposed by Hardisky et al. [52] and was perhaps the first to propose a moisture-based index using ρ_{NIR} and ρ_{SWIR1}, formulated as $(\rho_{NIR} - \rho_{SWIR1})/(\rho_{NIR} + \rho_{SWIR1})$. The results showed that the decrease of II in the canopy is correlated with the increasing salinity of soil in salt forests. This plot of water content shows a significant decrease in canopy moisture with increasing soil salinity. In summary, a combination of NDVI and II can detect morphological and physiological changes associated with moisture stress. However, using longer wavelengths is a more direct indicator of water content.

The normalized difference water index (NDWI) was proposed by Gao [47] based on research using moderate resolution imaging spectrometer (MODIS) and airborne visible infrared imaging spectrometer (AVIRIS) images to monitor vegetation changing based on the liquid water content in the canopy. The NDWI is originally formulated as $(\rho(0.86\,\mu\text{m}) - \rho(1.24\,\mu\text{m}))/(\rho(0.86\,\mu\text{m}) + \rho(1.24\ \ \text{I}\,\mu\text{m}))$. The vegetation index has been widely applied to Landsat images, especially in mangrove research, thus the index, universally, is formulated as $(\rho_{NIR} - \rho_{SWIR1})/(\rho_{NIR} + \rho_{SWIR1})$. The liquid water absorption in ρ_{NIR} is negligible and presents absorption at ρ_{SWIR}. Vegetation canopy scattering enhances water absorption. As a result, NDWI is sensitive to changes in the liquid water content of vegetation canopies. Atmospheric aerosol scattering effects from the ρ_{NIR} to ρ_{SWIR1} wavelength region are weak, so NDWI is less sensitive to the atmospheric effect than NDVI. However, NDWI does not completely remove the effect of soil background, but by increasing the vegetation fraction, the NDWI value increases. Tucker [40] first suggested that the ρ_{SWIR1} wavelength was the best-suited band for monitoring the water status at the plant canopy from space.

Normalized difference moisture index (NDMI) [53] is formulated $(\rho_{NIR} - \rho_{SWIR1})/(\rho_{NIR} + \rho_{SWIR1})$. However, retaining the term moisture, there is no better term, but the point is related to the wetness that includes the water content of vegetation, water absorbance in the fresh leaf, and soil wetness that will affect the sensitivity to soil and plant moisture. The difference between ρ_{NIR} and ρ_{SWIR1} appears in the ability of ρ_{SWIR1} wavelengths to absorb water, so that the index value can be used to estimate water content in the vegetation [54]. In the green leaves, the ρ_{NIR} band has more reflectance than the other bands, and the reduction in ρ_{SWIR1} reflectance compared to ρ_{NIR} is due to water absorption. Wetness change is a good indicator and the single most consistent indicator of forest change, including lighter disturbance/partial cuts, because it captures changes in ρ_{SWIR1}.

Mangrove discrimination indices (MDI) [34] intended to separate mangrove and nonmangrove vegetation using ρ_{NIR} and ρ_{SWIR1} or ρ_{SWIR2} and formulated as $(\rho_{NIR} - \rho_{SWIR1})/(\rho_{SWIR1})$. In his findings, ρ_{SWIR1} or ρ_{SWIR2} can increase the difference between mangrove and non-mangrove vegetation. In the application, when using MDI1 (ρ_{NIR} and ρ_{SWIR1}) to separate between mangroves and other vegetation, it is not yet clear whether it is best to move to MDI2 with the replacement from ρ_{SWIR1} to ρ_{SWIR2}.

All existing vegetation indices (VIs) and the formulas proposed by previous researchers are presented in Table 3.

2.2.4. Spectral Response of Segara Anakan Mangrove Vegetations as a Reference. Something is quite interesting in the mangrove environment of Segara Anakan, Cilacap, Central Java, Indonesia (Figure 1), reported by Winarso and Purwanto [55]. In the logged mangrove areas, shrubs such as *Derris trifoliata* and *Acanthus illicifolius* close the felled mangrove area so that the existing mangrove seedlings and saplings cannot develop. It is known that these shrubs are closely related and included in the mangrove association [56]. Using NDVI analysis, these shrubs show a very high index and even exceed the true mangrove due to strongly reflecting the ρ_{NIR}. Anyone who is not careful will be deceived, as if it is like dense mangroves.

The authors identified spectral responses in seven different land cover types surrounding the Segara Anakan mangroves, i.e., shrubs, Nypa, rice fields, land forest, mangroves, settlements, and waters. Each consists of ten plots recorded in the corrected Landsat 8 OLI image. The average spectral response of each land cover is shown in Figure 2(b).

The spectral response was collected from various features in Segara Anakan mangrove forests in the Landsat 8 OLI corrected images to create the automatic formula to separate mangrove and nonmangrove vegetation and other features.

2.2.5. Index Accuracy Assessment. The accuracy assessment of the research results consists of 2 stages: the spatial extent accuracy and the canopy density index assessments. The extent and boundary of mangroves with other vegetation will be visually clear using the RGB composite image of ρ_{NIR}-ρ_{SWIR1}-ρ_{Red}. The problem is how to automatically trace and capture what visually looks like a mangrove through an algorithm. In this research, the mangrove map is a map of mangroves as a mangrove community in the form of a tree community, from very sparse, which can be recorded in the image, to dense canopies. It cannot capture shrubs that are usually a part of the mangrove associated with the ecosystem. Similarly, the canopy index is a relative index that does not use the number of trees within a certain area. Classified as a dense index/the high index is the high value captured in the pixels as a spectral response from the execution of an algorithm.

The accurate assessment of the canopy density index in the study uses 200 randomly distributed points. It uses simple statistical methods to determine the linear relationship between the index created by this algorithm versus the indexes created by several previous vegetation indices.

3. Results and Discussion

3.1. Developing Formula for Mangrove. Based on the features characteristic of the spectral response as illustrated in Figure 2, extracted mangrove information can be designed and

Table 3: Summaries of the existing vegetation indices (Vis) and the formulas.

VI's	*Formula based on chlorophyll content*	*Reference*
RVI	(ρ_{Red}/ρ_{NIR})	[45]
NDVI	$(\rho_{N-R}-\rho_{Red})/(\rho_{NIR}+\rho_{Red})$	[46]
PVI	$2.5*(\rho_{N-R}-\rho_{Red})$	[48]
SAVI	$1.5*(\rho_{N-R}-\rho_{Red})/(\rho_{NIR}+\rho_{Red}+0.5)$	[49]
ARVI	$(\rho_{N-R}-(2*\rho_{Red})+\rho_{Blue})/(\rho_{NIR}+(2*\rho_{Red})+\rho_{Blue})$	[50]
VI's	*Formula based on water content*	*Reference*
II	$(\rho_{N-R}-\rho_{SWIR1})/(\rho_{NIR}+\rho_{SWIR1})$	[52]
NDWI	$(\rho_{N-R}-\rho_{SWIR1})/(\rho_{NIR}+\rho_{SWIR1})$	[47]
NDMI	$(\rho_{N-R}-\rho_{SWIR1})/(\rho_{NIR}+\rho_{SWIR1})$	[53]
MDI1/MDI2	$(\rho_{N-R}-\rho_{SWIR1})/(\rho_{SWIR1})$ and $(\rho_{N-R}-\rho_{SWIR2})/(\rho_{SWIR2})$	[34]

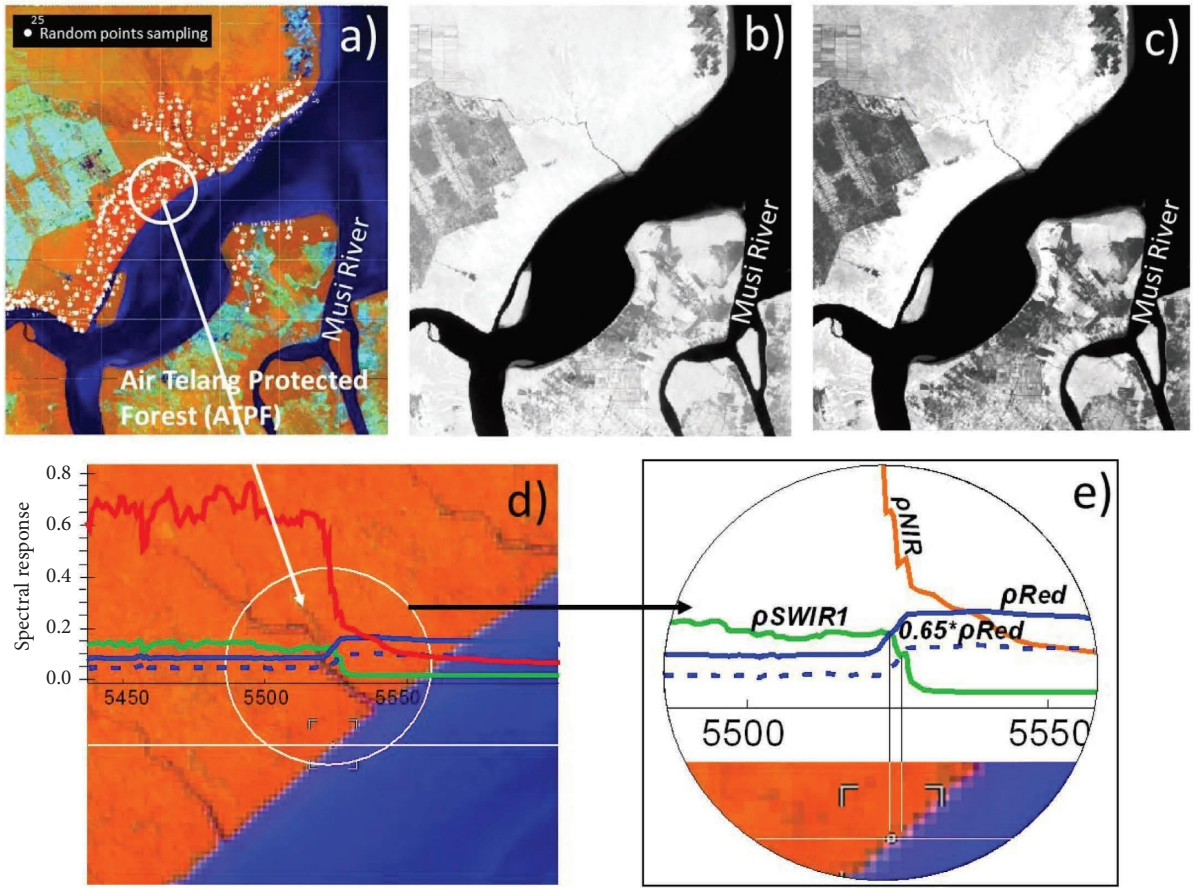

Figure 3: (a) RGB composite ρ_{NIR}-ρ_{SWIR1}-ρ_{Red} with 200 random points to assess the index. (b) A map of NDVI to decrease the spectral response of the water objects. (c) A map of slightly modified NDVI (in equation (2)) to get the forests by reducing the reflectance responses of other features. (d) RGB composite of ρ_{NIR}-ρ_{SWIR1}-ρ_{Red} in Landsat 8 OLI using constant $0.65*\rho_{Red}$ to avoid indefinite value in the 1 pixel towards the sea to obtain an index that is appropriate for the actual conditions. (e) Zoomed-in image of d.

calculated from other green vegetation using all the information attached to the satellite images. In the paper, the boundary of the mangrove vegetation index is examined using the canopy closure approach. Vegetation, soil, water, and seasonal and diurnal intertidal interactions are essential features that contribute to the pixel composition of mangroves in satellite remotely sensed images [31]. Mangrove presence becomes sharper in the Landsat image when displayed through an RGB (Red-Green-Blue) composite of $\rho_{NIR}-\rho_{SWR1}-\rho_{Red}$, as shown in Figure 3(a). However, the problem is how to automatically capture spatial extent as shown in the visual appearance. The properties of the vegetation will reflect ρ_{NIR} strongly, while ρ_{Red} plays an essential role in determining vegetation due to photosynthetic activities and ρ_{SWIR1} sensitivity to evaporation, the liquid water content in the leaf, and tidal inundation [31, 47, 55, 57–59]. In dense mangroves, ρ_{SWIR1} will be slightly higher than ρ_{Red} but will change twice as high in in nonmangroves (Figure 2(b)).

Similarly, in the nonmangrove, ρ_{NIR} is high but gradually decreases in mangroves and is absorbed in the water. Based on these spectral characteristics, it is possible to separate

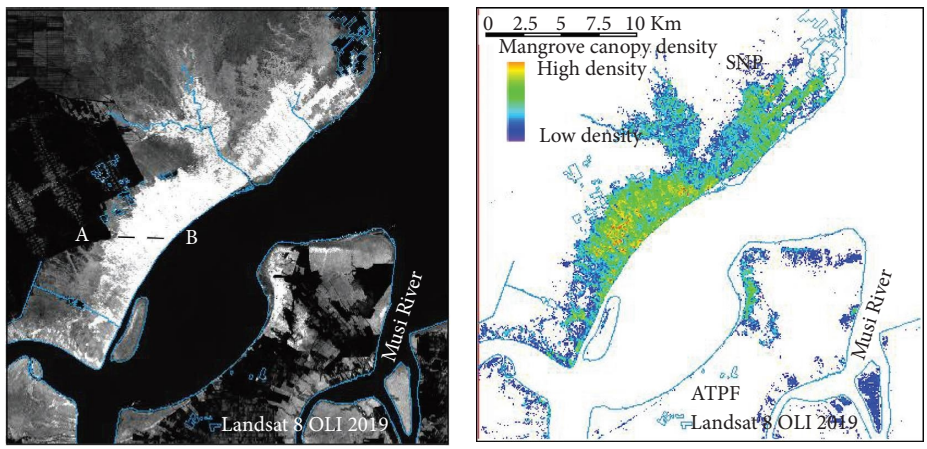

(a) (b)

Figure 4: (a) Image one band of the AMMI algorithm on a Landsat 8 OLI corrected image, and white pixels show the distribution of mangrove; A–B is an intersected line showing the spectral response between mangrove and nonmangrove. (b) The magnitude of the spectral response in the spectral color.

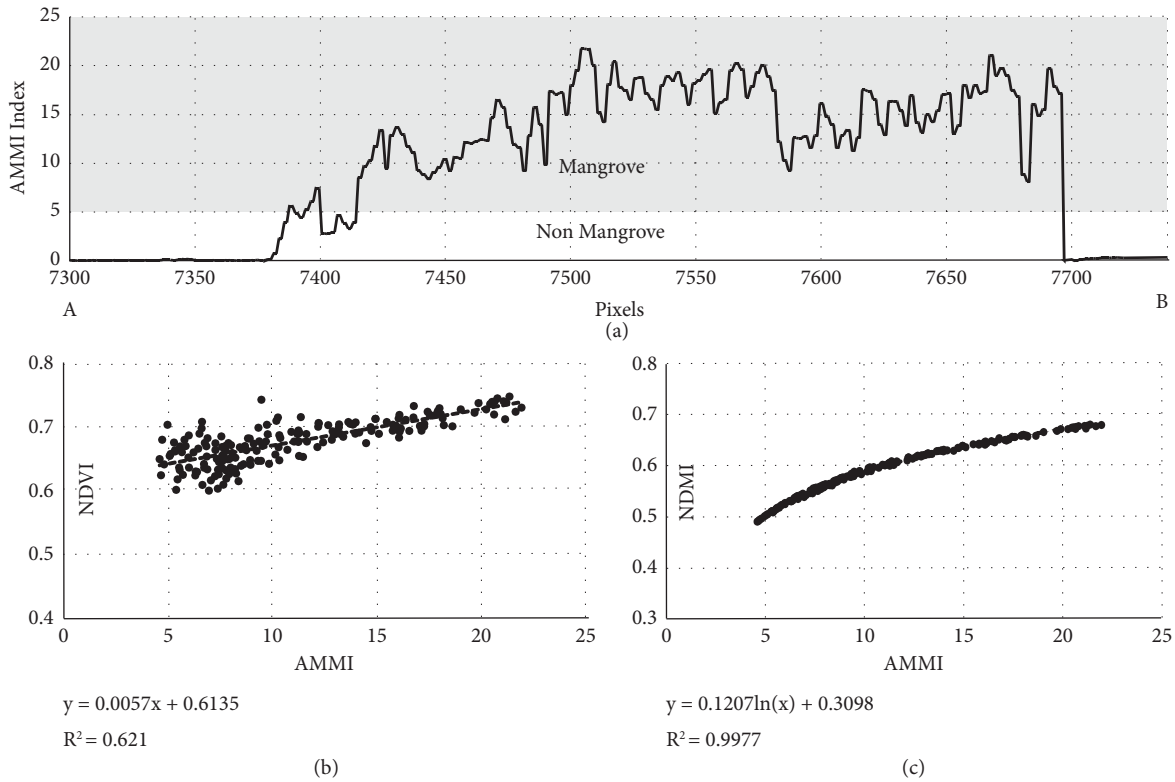

Figure 5: (a) The magnitude of AMMI spectral response through the A–B transect line is in Figure 4(a). (b) A linear correlation of the canopy index diagram between AMMI versus NDVI, and (c) AMMI versus NDWI through more than 200 randomly distributed points in Figure 3(a).

mangroves from other nonmangroves using a combination of ρ_{NIR}, $\rho_{SWIR1,}$ and ρ_{Red} reflectances. The normalized difference water index (NDWI) [60] is used to delineate and sharpen the water features (inland and open waters) and reduce the spectral reflectances of feature elements in the land. This index is applicable in identifying mangroves because of the liquid water component in the leaf canopy. Likewise, NDVI [46] can also be used as a basis for delineating land and eliminating/weakening the spectral of marine features.

Based on Figure 2, therefore, to create the mangrove maps, there are two steps. The first is delineating the land boundary by increasing the spectral forest vegetation and weakening/eliminating the spectral response of other non-forest areas. The second is tracing and capturing the mangroves on the land.

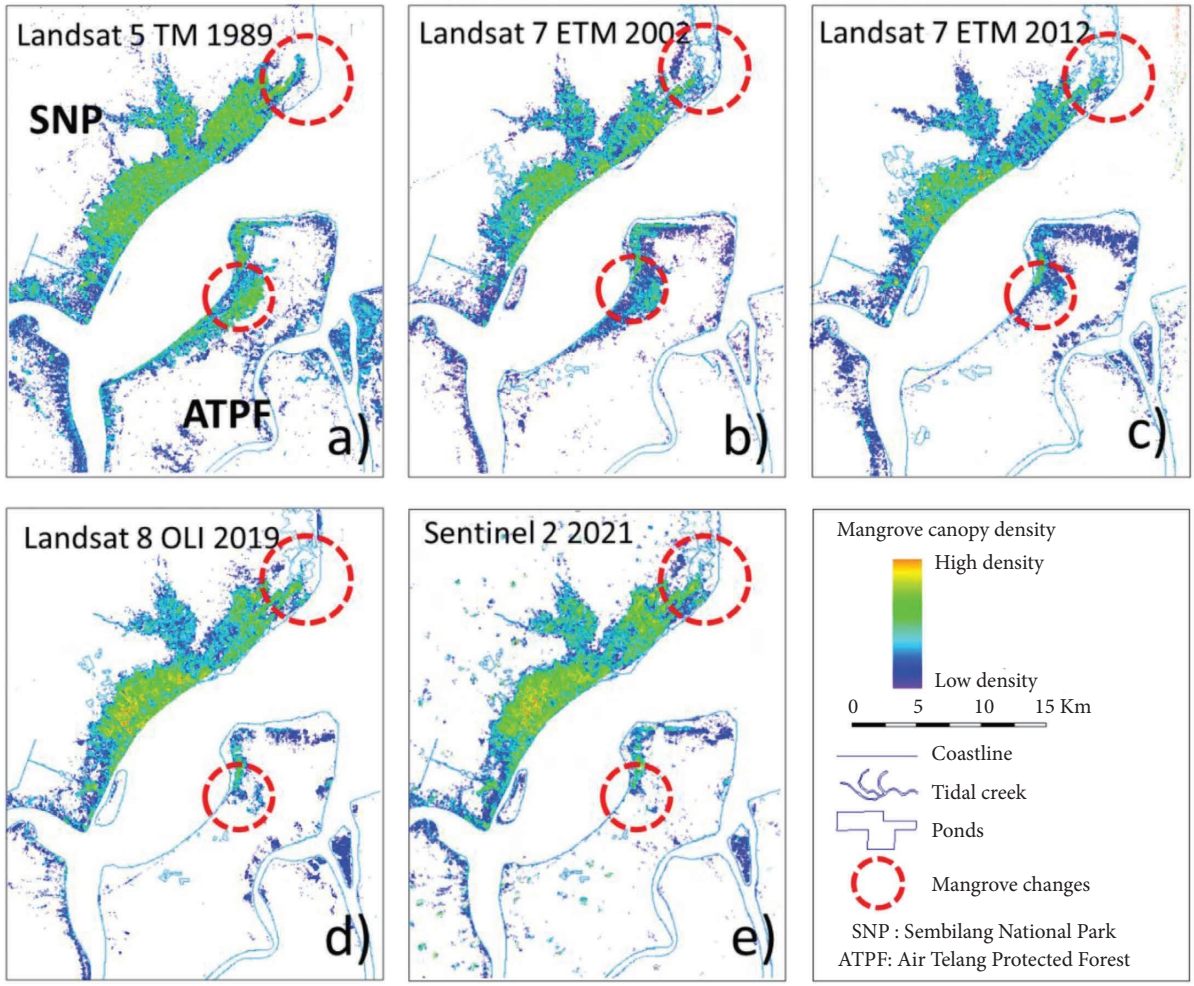

Figure 6: Maps of mangrove changes in the research area, 1989–2021. (a) Mangrove map in 1989 using Landsat 5 TM, (b) and (c) mangrove map in 2002 and 2012 using Landsat 7 ETM, (d) mangrove map in 2019 using Landsat 8 OLI, and (e) mangrove map in 2021 using Sentinel 2.

3.1.1. Improve the Spectral Response of Vegetation. The first step aims to improve the spectral response of vegetation (land forests and mangroves) while reducing/weakening the spectral response of marine objects (water, coral, and mud), shrubs, settlements, and open land. Although the NDVI formula can capture land and eliminate water features, it is less accurate in distinguishing land vegetation. At this step, it is necessary to preserve vegetation features while ignoring other features, hence the slight modification of the NDVI formula by replacing the ρ_{NIR} in the denominator with ρ_{SWIR1}. This will effectively improve the spectral response for both land and mangrove forests. To trace the land vegetation using ρ_{Red}, ρ_{NIR}, and ρ_{SWIR1} in the following equation:

$$\frac{(\rho_{\mathrm{NIR}} - \rho_{\mathrm{Red}})}{(\rho_{\mathrm{Red}} + \rho_{\mathrm{SWIR1}})}. \tag{2}$$

As known, ρ_{NIR} is sensitive to all vegetation types, but the greater part will be absorbed in the water environment. Likewise, ρ_{Red} will show lower reflectance in the vegetation environment due to chlorophyll absorption and higher reflectance in the water environment.

The combination of ρ_{Red} and ρ_{NIR}, referring to the spectral response in Figure 3(b), cannot separate mangrove forests from terrestrial forests because they have the same spectral value. It would be more effective to use ρ_{SWIR1} which has different index ranges and is longer. Figure 3(c) compares the sharpness of separating the forest canopy from other vegetation, including shrubs, by replacing ρ_{SWIR1} in the denominator with ρ_{Red} in the NDVI formula.

3.1.2. Identification and Tracing of Mangroves. The difference in ρ_{SWIR1} index between the mangrove and non-mangrove forest is thought to be a difference in water content or moisture in the forest canopy. To trace the mangrove extent is by using ρ_{NIR}, ρ_{SWIR1}, and ρ_{Red} in the following equation:

$$\frac{(\rho_{\mathrm{NIR}} - \rho_{\mathrm{SWIR1}})}{(\rho_{\mathrm{SWIR1}} - 0.65 * \rho_{\mathrm{Red}})}. \tag{3}$$

The constant of 0.65 in equation (3) reduces the ρ_{Red} reflectance to avoid the infinite value in the mangrove edge bordering the sea. In the outer mangrove, when mangroves

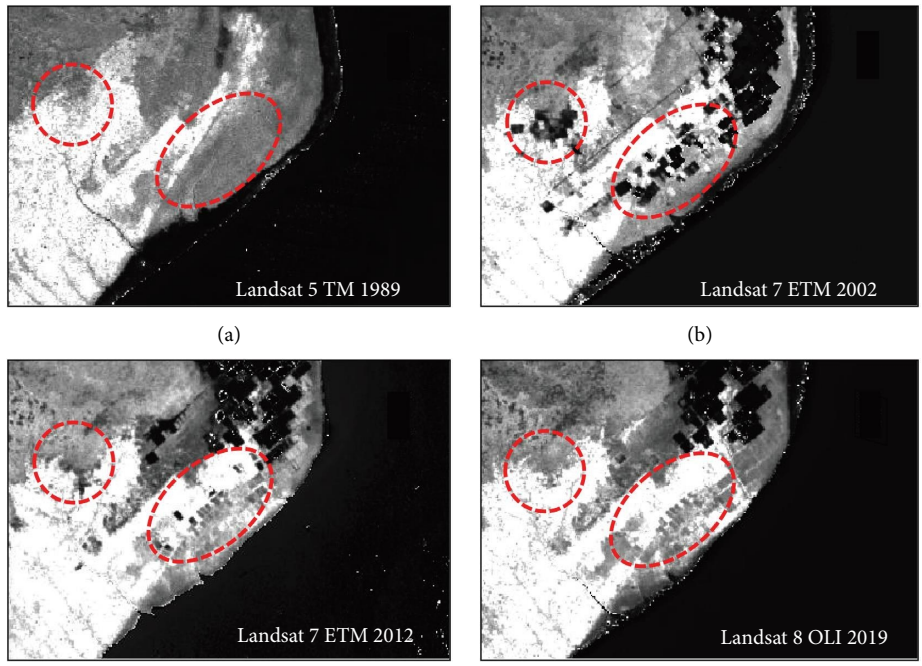

Figure 7: Mangrove condition using the AMMI algorithm 1989–2019; and the red circle shows the dynamics of change. (a) Mangrove condition in 1989, (b) Mangrove logging marks in 2002, (c) Abandoned logging in 2012, and (d) Mangroves have not completely closed the former ponds recorded in the 2019 image. Active ponds are currently outside the mangrove.

border the sea, the index of 1 pixel will be overestimated because ρ_{SWIR1} is lower than ρ_{Red} (Figure 3(d) and zoomed in Figure 3(e)). the intensity of the ρ_{Red} to obtain a more precise boundary is reduced and an index that is appropriate for the actual conditions.

Based on the two equations, the automatic mangrove map and index (AMMI) in this study can be written as follows:

$$\frac{(\rho_{\mathrm{NIR}} - \rho_{\mathrm{Red}})}{(\rho_{\mathrm{Red}} + \rho_{\mathrm{SWIR1}})} * \frac{(\rho_{\mathrm{NIR}} - \rho_{\mathrm{SWIR1}})}{(\rho_{\mathrm{SWIR1}} - 0.65 * \rho_{\mathrm{Red}})}. \quad (4)$$

The results of AMMI execution using the combination of ρ_{Red},ρ_{NIR}, and ρ_{SWIR1} in radiometrically corrected Landsat 8 OLI, September 9, 2019, trace and capture the spatial extent and present the relative canopy density of the mangrove in one band of the grayscale image is shown in Figure 4(a). The magnitude of the spectral response in the spectral color is shown in Figure 4(b). The figures show that mangroves will reflect a stronger spectral response, while nonmangrove features will be weaker.

3.2. Accuracy Assessment. Spatially, the AMMI captures the mangroves from sparse mangroves, indicated by the low spectral sensitivity with an index of about 5, to dense mangroves (>20), as shown in Figure 5(a), and the index below 5 is classified as nonmangrove. The relationship of the index to the NDVI, using 200 randomly distributed points (Figure 3(a)), has a correlation value (R^2) of 0.62 (Figure 5(b)), and the relationship to NDWI/NDMI shows a very high correlation value, even reaching 0.99 (Figure 5(c)). As is well known, NDWI/NDMI were initially created and applied for the terrestrial forest, but it was also explained that forest canopy density from satellite imagery is closely related to the water content in the canopy.

3.3. Monitoring Mangrove Changes Using Multitemporal Images. To study the evolution of mangroves chronologically and monitor their condition, the AMMI performs well in detecting mangrove changes. Various satellite images can be used, namely Landsat 5 TM 1989 (Figure 6(a)), Landsat 7 ETM 2002 and 2012 (Figures 6(b) and 6(c)), Landsat 8 OLI 2019 (Figure 6(d)), and even Sentinel 2 2021 (Figure 6(e)). Figure 6(e) shows this was an inset, a small clip from a high-spatial-resolution Google satellite to evaluate the algorithm's performance. The accuracy of the mangrove extent is comparable to the high resolution of Google's satellite 2022 covering the research area. AMMI only showed the spectral response of mangroves and eliminated other spectral responses such as shrubs, settlements, dry land, or forest land.

The spatial accuracy of AMMI in capturing and trapping the mangrove changes will be clearer, as shown in Figure 7. Figure 7(a) depicts the initial conditions before the SNP mangroves were damaged. Changes in mangroves in the SNP area are generally caused by logging/felling to create ponds/aquaculture and typically bloom between 1989 and 2002, as illustrated in Figure 7(b). A symmetrical square felling pattern determined the conversion to ponds. However, in the following imagery (Figure 7(c)), many of these ponds have been abandoned and converted back to mangrove forests, and Figure 4(d) shows mangroves restored to

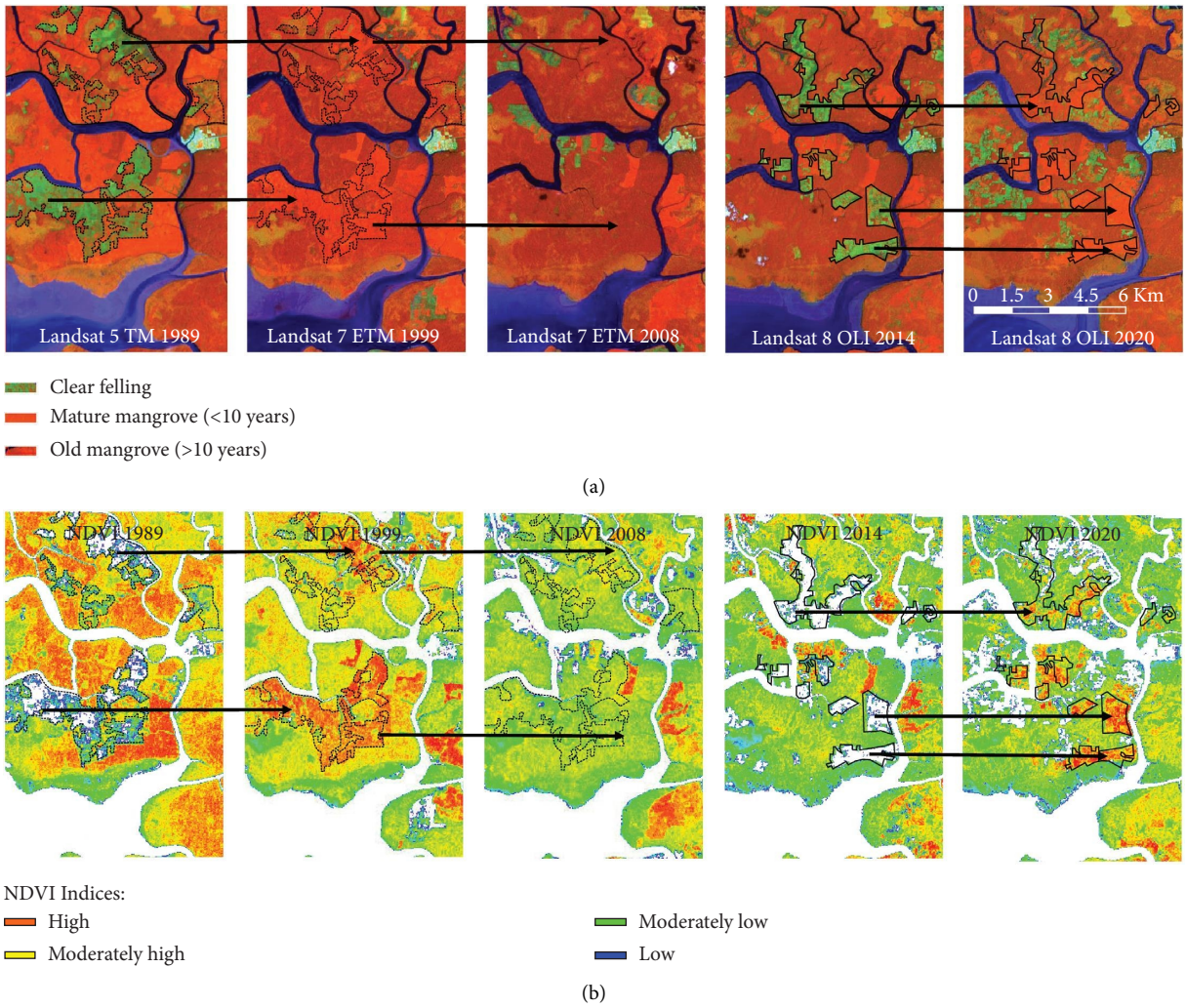

Figure 8: (a) It shows the chronology of the harvesting process, replanting, and growth in a production mangrove forest in Matang, Malaysia, using Landsat 5TM, Landsat 7 ETM, and Landsat 8 OLI time series through $\rho_{NIR} - \rho_{SWIR1} - \rho_{Red}$ of RGB composite image. (b) Changes and shifts in NDVI according to the age of mangroves are shown.

their pre-establishment condition. Some active ponds are found outside the mangrove forest.

The correlation value between AMMI and NDWI/NDMI reached 0.99, indicating that the AMMI's performance is comparable to that of the NDWI/NDMI index. Based on these results, AMMI is a breakthrough in NDWI/NDMI automatic innovation that automatically traces and captures mangroves and informs the index.

3.4. Learn about Mangrove Changes from the Mangrove Production Forests. NDWI/NDMI vegetation indices in the mangrove research are less commonly used than NDVI. However, NDWI/NDMI has many advantages, including quickly identifying minor damage and light disturbances. According to Otero et al. [61], mangrove age from sprout to 7 years old will correlate with a sharply increasing NDWI/NDMI index. More than seven years old are no longer correlated and are frequently reduced. This finding is valuable because their research was in Matang Mangrove Forest Reserve (MMFR), Malaysia, one of the mangrove production forests rarely found in the mangrove forests in the world. Further research revealed that reducing the NDWI index at mature to old age in mangroves was caused by the gaping process of the canopy. Will the index shift in mangroves from maturity to old age occur when using another index, such as NDVI. Goessens et al. [62] reported the status of mangrove forest production in Matang, Malaysia, located at 4.82 N and 100.59 E, providing an exciting research location for studying the evolution of mangroves.

To avoid breaking the code of ethics and infringing on the rights of neighboring countries, the authors describe at a glance a small part of Malaysia's Matang mangrove forest using multi-temporal Landsat images, as shown in Figure 8. The images show how new mangroves grow and develop after harvesting. When these young mangroves are 7–10 years old, they have the highest NDVI values; however, as mangroves age, their NDVI values decrease, and the highest values shift to other younger mangroves, and so on. Noda et al. [63]

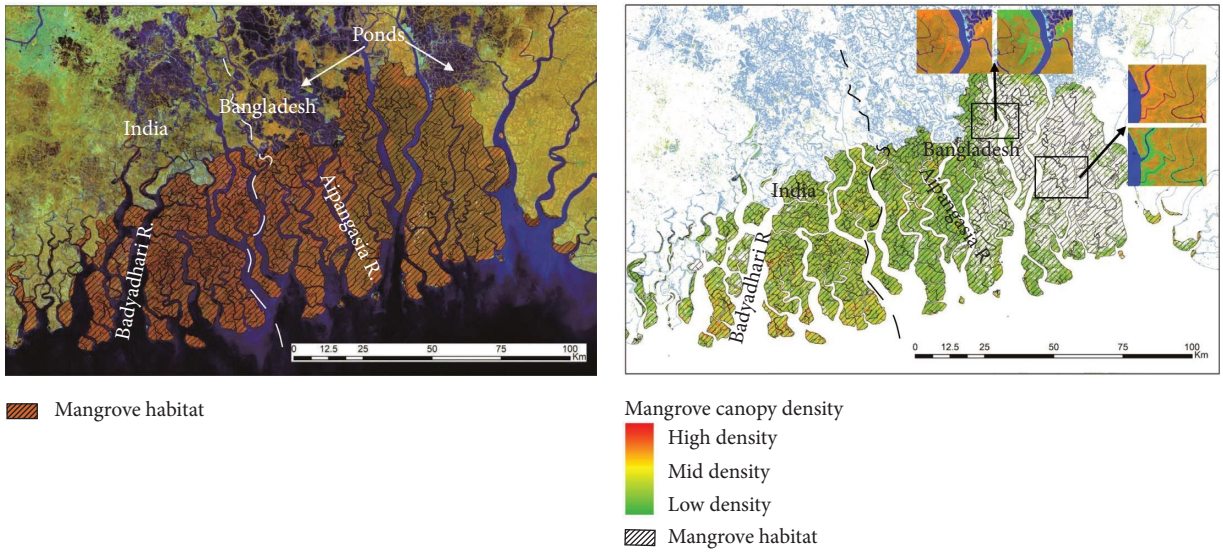

Figure 9: (a) Surface reflectance of NIR-SWIR-Red composite image of Landsat 8, 2021 Sundarban mangrove forest (India and Bangladesh) downloaded using the GEE platform and (b) Mangrove map of Sundarban mangrove forest (India and Bangladesh) using AMMI algorithm.

investigated the high NDVI in young vegetation, which has a bright green color, ρ_{Green} increased after leaf emergence and decreased after canopy closure during early growth, while ρ_{Red} continued to decline. According to these findings, the highest NDVI is not always found in the most densely forested mangroves, nor is it always found in the oldest and healthiest mangroves. NDVI levels are typically highest in mature mangroves aged 7 to 10 years. Furthermore, as seen in NDWI/NDMI, the NDVI decreases slightly with increasing mangrove age while remaining in the moderately high range.

Besides detecting damage due to logging, NDMI is also sensitive to forest disturbances caused by diseases related to forest health. Reference [64] and vegetation damage due to drought effects [65]; it is also beneficial to monitor water status as an early warning against drought [66].

3.5. Application of AMMI in a Broader Area Using the GEE Facilities. In applying automatic mangrove mapping to a larger area, the GEE facility was used to reveal the Sundarban mangrove forest, stretching from eastern India to Bangladesh, using surface reflectance of Landsat 8, 2021 imagery. Based on visual interpretation informs, the Sundarbans mangrove habitat area of 621925 ha is divided into India (214769 ha) and Bangladesh (407156 ha) (Figure 9(a)).

Analysis using the AMMI algorithm shows that the true mangrove in Sundarban India is 183296 ha (85% of habitat), while that in Sundarban Bangladesh is only 189733 ha (47%). Sundarban Bangladesh mangroves are sparsely distributed and concentrated only around rivers, with a very low canopy density and are inhabited mainly by shrubs and open land (Figure 9(b)).

The Sundarban mangrove has become an icon of the world's largest mangroves. Is there any donor agency that intends to replant and reforest Sundarban mangroves in Bangladesh?

4. Conclusion

The AMMI application in mangrove mapping in Musi Delta, South Sumatra, Indonesia, based on the spatial distribution and the index of canopy density using Landsat 5 TM, Landsat 7 ETM, Landsat 8 OLI, and Sentinel 2 performs well. The mangrove extent has been spatially traced and captured, corresponding to and matching the visual satellite images. The canopy density index of AMMI versus NDVI has a correlation value (R^2) of 0.62 in correlation diagrams, and AMMI versus NDWI/NDMI has a significant value with an R^2 of 0.99.

The paper revealed how to automatically trace and capture mangroves for future research and eliminate manual digitizing, which is exhausting and time-consuming and frequently results in inaccuracy due to misinterpretation. Operationally, it is simple to use, produces mangrove maps quickly, and efficiently monitors the mangrove condition from time to time. The instantaneous application may be sufficient for monitoring mangrove conditions in protected mangrove forests by local communities, practitioners, and conservationists.

Scientifically, for future research, mapping of mangroves over a larger area and describing the surrounding physical environment is the baseline data for the mangrove condition. Other supporting data, such as tree density and their age per unit area, biota content statistics, and geo-biochemical data, will determine the mangrove health index.

Data Availability

Data are available in Supplementary.

Conflicts of Interest

The authors declare that they have no conflicts of interest.

Authors' Contributions

Suyarso conducted all the experiments and research design, and Praditya Avianto reviewed and analyzed the Sundarban Mangroves in India and Bangladesh using the Google Earth Engine platform.

Acknowledgments

This work was partially funded by the Coral Reef Rehabilitation and Management Program—Coral Triangle Initiative (COREMAP—CTI) Project and partially by the authors. The authors would like to express their gratitude to Dr. Martiwi Diah Setyawati, Dr. Yaya Ihya Ulumuddin, and Bayu Prayudha (doctor candidate) for their discussions, criticisms, suggestions, and assistance in developing the automatic mangrove map. The authors also thank all the Marine Geospatial Laboratory colleagues at the Research Center for Oceanography, National Research and Innovation Agency, for providing the infrastructure needed to prepare the manuscript.

Supplementary Materials

Appendix: Data to assess the correlation index of AMMI to NDVI and NDWI. (*Supplementary Materials*)

References

[1] C. D. Field, "Impact of expected climate change on mangroves," *Hydrobiologia*, vol. 295, no. 1–3, pp. 75–81, 1995.

[2] K. Kathiresan and B. L. Bingham, "Biology of mangroves and mangrove ecosystems," *Advances in Marine Biology*, vol. 40, pp. 81–251, 2001.

[3] I. Nagelkerken, S. J. M. Blaber, S. Bouillon et al., "The habitat function of mangroves for terrestrial and marine fauna: a review," *Aquatic Botany*, vol. 89, no. 2, pp. 155–185, 2008.

[4] R. Costanza, R. d'Arge, R. de Groot et al., "The value of the world's ecosystem services and natural capital," *Nature*, vol. 387, no. 6630, pp. 253–260, 1997.

[5] M. Hutomo and M. K. Moosa, "Indonesian marine and coastal biodiversity: present status," *Indian Journal of Marine Sciences*, vol. 34, no. 1, pp. 88–97, 2005.

[6] S. Srikanth, S. K. Y. Lum, and Z. Chen, "Mangrove root: adaptations and ecological importance," *Trees*, vol. 30, no. 2, pp. 451–465, 2016.

[7] D. C. Donato, J. B. Kauffman, D. Murdiyarso, S. Kurnianto, M. Stidham, and M. Kanninen, "Mangroves among the most carbon-rich forests in the tropics," *Nature Geoscience*, vol. 4, no. 5, pp. 293–297, 2011.

[8] L. Carugati, B. Gatto, E. Rastelli et al., "Impact of mangrove forests degradation on biodiversity and ecosystem functioning," *Scientific Reports*, vol. 8, no. 1, Article ID 13298, 2018.

[9] T. E. Fatoyinbo, M. Simard, R. A. Washington-Allen, and H. H. Shugart, "Landscape-scale extent, height, biomass, and carbon estimation of Mozambique's mangrove forests with Landsat ETM+, and shuttle radar topography mission elevation data," *Journal of Geophysical Research: Biogeosciences*, vol. 113, no. G2, 2008.

[10] P. Wicaksono, P. Danoedoro, Hartono, and U. Nehren, "Mangrove biomass carbon stock mapping of the Karimunjawa Islands using multispectral remote sensing," *International Journal of Remote Sensing*, vol. 37, no. 1, pp. 26–52, 2016.

[11] A. W. Hastuti, K. I. Suniada, and F. Islamy, "Carbon stock estimation of mangrove vegetation using remote sensing in Perancak Estuary, Jembrana District, Bali," *International Journal of Remote Sensing and Earth Sciences (IJReSES)*, vol. 14, no. 2, pp. 137–150, 2018.

[12] J. Sanderman, T. Hengl, G. Fiske et al., "A global map of mangrove forest soil carbon at 30 m spatial resolution," *Environmental Research Letters*, vol. 13, no. 5, Article ID 055002, 2018.

[13] A. R. Jones, R. Raja Segaran, K. D. Clarke, M. Waycott, W. S. H. Goh, and B. M. Gillanders, "Estimating mangrove tree biomass and carbon content: a comparison of forest inventory techniques and drone imagery," *Frontiers in Marine Science*, vol. 6, p. 784, 2020.

[14] M. Wang, W. Cao, Q. Guan, G. Wu, and F. Wang, "Assessing changes of mangrove forest in a coastal region of southeast China using multi-temporal satellite images," *Estuarine, Coastal and Shelf Science*, vol. 207, pp. 283–292, 2018.

[15] FAO (Food and Agriculture Organisation) of the United Nation 2005, The world's mangroves 1980–2005, FAO Forestry Paper, 153, http://www.fao.org/3/a1427e/a1427e00.pdf.

[16] C. Giri, E. Ochieng, L. L. Tieszen et al., "Observation and monitoring of mangrove forests using remote sensing: opportunities and challenges," *Remote Sensing*, vol. 8, no. 9, pp. 783–159, 2011.

[17] N. C. Duke, J.-O. Meynecke, S. Dittmann et al., "A world without mangroves?" *Science*, vol. 317, no. 5834, pp. 41-42, 2007.

[18] K. D. Kanniah, A. Sheikhi, A. P. Cracknell et al., "Satellite images for monitoring mangrove cover changes in a fast growing economic region in Southern Peninsular Malaysia," *Remote Sensing*, vol. 7, no. 11, pp. 14360–14385, 2015.

[19] D. M. Alongi, "Present state and future of the world's mangrove forests," *Environmental Conservation*, vol. 29, no. 3, pp. 331–349, 2002.

[20] I. Valiela, J. L. Bowen, and K. York, "Mangrove forests: one of the world's threatened major tropical environments," *BioScience*, vol. 51, no. 10, pp. 807–815, 2001.

[21] L. Chen, W. Wang, Y. Zhang, and G. Lin, "Recent progresses in mangrove conservation, restoration and research in China," *Journal of Plant Ecology*, vol. 2, no. 2, pp. 45–54, 2009.

[22] B. K. Veettil, R. D. Ward, N. X. Quang, N. T. T. Trang, and T. H. Giang, "Mangroves of Vietnam: historical development, current state of research and future threats," *Estuarine, Coastal and Shelf Science*, vol. 218, pp. 212–236, 2018.

[23] S. Soemodihardjo, Soeroyo, and Suyarso, "The mangrove forest of Segara Anakan: an assessment of their condition and prospect," in *Proceedings of the International Center for Living Aquatic Resources Management (ICLARM) Conference Proceedings*, Makati City, Philippines, 1994.

[24] M. D. M. R. B. Taylor, J. L. Rangel-Salazar, and B. C. Hernández, "Resilience in a Mexican Pacific mangrove after hurricanes: implications for conservation-restoration," *Journal of Environmental Protection*, vol. 04, no. 12, pp. 1383–1391, 2013.

[25] M. S. Ross, P. L. Ruiz, J. P. Sah, D. L. Reed, J. Walters, and J. F. Meeder, "Early post-hurricane stand development in Fringe mangrove forests of contrasting productivity," *Plant Ecology*, vol. 185, no. 2, pp. 283–297, 2006.

[26] N. Brooks, *Vulnerability, Risk and Adaptation: A Conceptual Framework*, p. 20, Tyndall Centre for Climate Change Research, University of East Anglia, Norwich, UK, 2003.

[27] E. L. Gilman, J. Ellison, N. C. Duke, and C. Field, "Threats to mangroves from climate change and adaptation options: a review," *Aquatic Botany*, vol. 89, no. 2, pp. 237–250, 2008.

[28] P. C. Sierra-Correa and J. R. Cantera Kintz, "Ecosystem-based adaptation for improving coastal planning for sea-level rise: a systematic review for mangrove coasts," *Marine Policy*, vol. 51, pp. 385–393, 2015.

[29] ITTO (International Tropical Timber Organisation); Ministry of environment and Forestry of Indonesia; international society for mangrove ecosystems. International Conference on Sustainable Mangrove Ecosystems: Managing a Vital Resource for Achieving the Sustainable Development Goals and the Paris Agreement, Bali, 2017, https://www.itto.int/files/itto_project_db_input/3202/Competition/International_Mangrove_Conference_Report-English.pdf.

[30] M. Kamal, W. P. Hartono, N. S. Adi, and S. Arjasakusuma, "Assessment of mangrove forest degradation through canopy fractional cover in Karimunjawa, Central Java, Indonesia," *Geoplanning*, vol. 3, no. 2, pp. 107–116, 2016.

[31] C. Kuenzer, A. Bluemel, S. Gebhardt, T. V. Quoc, and S. Dech, "Remote sensing of mangrove ecosystems: a review," *Remote Sensing*, vol. 3, no. 5, pp. 878–928, 2011.

[32] P. P. Rhyma, K. Norizah, A. A. M. Ismail, and I. Shamsudin, "A review of uses of satellite imagery in monitoring mangrove forests," in *Proceedings of the 8thIOP Conference Series: Earth and Environmental Science*, vol. 37, Kuala Lumpur, Malaysia, 2016.

[33] L. Wang, M. Jia, D. Yin, and J. Tian, "A review of remote sensing for mangrove forests: 1956–2018," *Remote Sensing of Environment*, vol. 231, Article ID 111223, 2019.

[34] D. Wang, B. B. Wan, P. Qiu et al., "Evaluating the performance of Sentinel-2, Landsat 8 and Pléiades-1 in mapping mangrove extent and species," *Remote Sensing*, vol. 10, no. 9, p. 1468, 2018.

[35] C. D. Woodroffe, "Mangrove sediments and geomorphology," in *Tropical Mangrove Ecosystems*, A. I. Robertson and D. M. Alongi, Eds., pp. 7–41, Am. Geophys. Union, Washington, DC, USA, 1992.

[36] J. M. M. Yancho, T. G. Jones, S. R. Gandhi, C. Ferster, A. Lin, and L. Glass, "The Google earth engine mangrove mapping methodology (GEEMMM)," *Remote Sensing*, vol. 12, no. 22, p. 3758, 2020.

[37] H. Tamiminia, B. Salehi, M. Mahdianpari, L. Quackenbush, S. Adeli, and B. Brisco, "Google earth engine for geo-big data applications: a meta-analysis and systematic review," *ISPRS Journal of Photogrammetry and Remote Sensing*, vol. 164, pp. 152–170, 2020.

[38] B. Clark, J. Suomalainen, and P. Pellikka, "An historical empirical line method for the retrieval of surface reflectance factor from multi-temporal SPOT HRV, HRVIR and HRG multispectral satellite imagery," *International Journal of Applied Earth Observation and Geoinformation*, vol. 13, no. 2, pp. 292–307, 2011.

[39] L. T. Hauser, G. Nguyen Vu, B. A. Nguyen et al., "Uncovering the spatio-temporal dynamics of land cover change and fragmentation of mangroves in the Ca Mau peninsula, Vietnam using multi-temporal SPOT satellite imagery (2004–2013)," *Applied Geography*, vol. 86, pp. 197–207, 2017.

[40] C. J. Tucker, "Remote sensing of leaf water content in the near-infrared," *Remote Sensing of Environment*, vol. 10, no. 1, pp. 23–32, 1980.

[41] J. Peñuelas and I. Filella, "Visible and near-infrared reflectance techniques for diagnosing plant physiological status," *Trends in Plant Science*, vol. 3, no. 4, pp. 151–156, 1998.

[42] C. Zhang, Y. Liu, J. Kovacs, F. Flores-Verdugo, F. Flores-de-Santiago, and K. Chen, "Spectral response to varying levels of leaf pigments collected from a degraded mangrove forest," *Journal of Applied Remote Sensing*, vol. 6, no. 1, Article ID 063501, 2012.

[43] J. Xue and B. Su, "Significant remote sensing vegetation indices: a review of developments and applications," *Journal of Sensors*, vol. 2017, Article ID 1353691, 17 pages, 2017.

[44] N. Kobayashi, H. Tani, X. Wang, and R. Sonobe, "Crop classification using spectral indices derived from Sentinel-2A imagery," *Journal of Information and Telecommunication*, vol. 4, no. 1, pp. 67–90, 2020.

[45] C. F. Jordan, "Derivation of leaf-area index from quality of light on the forest floor," *Ecology*, vol. 50, no. 4, pp. 663–666, 1969.

[46] J. Rouse, R. Haas, D. Deering, J. A. Schell, and J. Harlan, "Monitoring vegetation systems in the great plains with ERTS," in *Proceedings of the 3rd ERTS-1 Symposium, NASA SP-351*, Washington, DC, USA, 1973.

[47] B. C. Gao, "NDWI A normalized difference water index for remote sensing of vegetation liquid water from space," *Remote Sensing of Environment*, vol. 58, no. 3, pp. 257–266, 1996.

[48] A. J. Richardson and C. Weigand, "Distinguishing vegetation from soil background information," *Photogrammetric Engineering & Remote Sensing*, vol. 43, no. 12, pp. 1541–1552, 1977.

[49] Y. J. Kaufman and D. Tanre, "Atmospherically resistant vegetation index (ARVI) for EOS-MODIS," *IEEE Transactions on Geoscience and Remote Sensing*, vol. 30, no. 2, pp. 261–270, 1992.

[50] A. R. Huete, "A soil-adjusted vegetation index (SAVI)," *Remote Sensing of Environment*, vol. 25, no. 3, pp. 295–309, 1988.

[51] B. Pinty and M. M. Verstraete, "GEMI: a non-linear index to monitor global vegetation from satellites," *Vegetation*, vol. 101, no. 1, pp. 15–20, 1992.

[52] M. A. Hardisky, V. Klemas, and R. M. Smart, "The influence of soil salinity, growth form, and leaf moisture on-the spectral radiance of *Spartina alterniflora* canopies," *Photogrammetric Engineering & Remote Sensing*, vol. 49, no. 1, pp. 77–83, 1983.

[53] E. H. Wilson and S. A. Sader, "Detection of forest harvest type using multiple dates of Landsat TM imagery," *Remote Sensing of Environment*, vol. 80, no. 3, pp. 385–396, 2002.

[54] F. J. Lozano, S. Suárez-Seoane, and E. de Luis, "Assessment of several spectral indices derived from multi-temporal Landsat data for fire occurrence probability modelling," *Remote Sensing of Environment*, vol. 107, no. 4, pp. 533–544, 2007.

[55] G. Winarso and A. D. Purwanto, "Evaluation on mangrove damage level based on Landsat 8 image," *International Journal of Remote Sensing and Earth Sciences*, vol. 11, no. 2, pp. 105–116, 2014.

[56] N. C. Duke and K. Schmitt, "Mangroves: unusual forests at the seas edge," in *Book: Tropical Forestry Handbook*, M. Köhl and L. Pancel, Eds., Springer, Berlin, Germany, pp. 1–24, 2015.

[57] M. Amani, B. Salehi, S. Mahdavi, and B. Brisco, "Spectral analysis of wetlands using multi-source optical satellite imagery," *ISPRS Journal of Photogrammetry and Remote Sensing*, vol. 144, pp. 119–136, 2018.

[58] S. Bhatnagar, L. Gill, S. Regan et al., "Mapping vegetation communities inside wetlands using Sentinel-2 imagery in Ireland," *International Journal of Applied Earth Observation and Geoinformation*, vol. 88, Article ID 102083, 2020.

[59] S. Thakur, I. Mondal, P. B. Ghosh, P. Das, and T. K. De, "A review of the application of multispectral remote sensing in the study of mangrove ecosystems with special emphasis on

image processing techniques," *Spatial Information Research*, vol. 28, no. 1, pp. 39–51, 2020.

[60] S. K. McFeeters, "The use of the normalized difference water index (NDWI) in the delineation of open water features," *International Journal of Remote Sensing*, vol. 17, no. 7, pp. 1425–1432, 1996.

[61] V. Otero, R. Van De Kerchove, B. Satyanarayana, H. Mohd-Lokman, R. Lucas, and F. Dahdouh-Guebas, "An Analysis of the early regeneration of mangrove forests using Landsat time series in the Matang mangrove forest reserve, Peninsular Malaysia," *Remote Sensing*, vol. 11, no. 7, p. 774, 2019.

[62] A. Goessens, B. Satyanarayana, T. Van der Stocken et al., "Is Matang mangrove forest in Malaysia sustainably rejuvenating after more than a century of conservation and harvesting management?" *PLoS One*, vol. 9, no. 8, Article ID e105069, 2014.

[63] H. M. Noda, H. Muraoka, and K. N. Nasahara, "Plant ecophysiological processes in spectral profiles: perspective from a deciduous broadleaf forest," *Journal of Plant Research*, vol. 134, no. 4, pp. 737–751, 2021.

[64] J. Lastovicka, P. Svec, D. Paluba et al., "Sentinel-2 data in an evaluation of the impact of the disturbances on forest vegetation," *Remote Sensing*, vol. 12, p. 1914, 2020.

[65] A. Sierra-Soler, J. Adamowski, Z. Qi, H. Saadat, and S. Pingale, "High accuracy land use land cover (LULC) maps for detecting agricultural drought effects in rainfed agro-ecosystems in central Mexico," *Journal of Water and Land Development*, vol. 26, no. 1, pp. 19–35, 2015.

[66] D. Marusig, F. Petruzzellis, M. Tomasella, R. Napolitano, A. Altobelli, and A. Nardini, "Correlation of field-measured and remotely sensed plant water status as a tool to monitor the risk of drought-induced forest decline," *Forests*, vol. 11, no. 1, p. 77, 2020.